designs

MDPI

Article

Prediction of Shear Strength in Anisotropic Structural Planes Considering Size Effects

Wei-Bin Ma [1,2], Wen-Hao Zou [1,2], Jin-Long Zhang [1,2] and Gan Li [3,*]

[1] Railway Engineering Research Institute, China Academy of Railway Sciences Corporation Limited, Beijing 100081, China; dwangfei@163.com (W.-B.M.); zouwenhao0308@163.com (W.-H.Z.); zjl525@outlook.com (J.-L.Z.)
[2] State Key Laboratory of High-Speed Railway Track System, Beijing 100081, China
[3] Institute of Rock Mechanics, School of Civil and Environmental Engineering and Geography Science, Ningbo University, Ningbo 315000, China
* Correspondence: ligan303@126.com; Tel.: +86-159-1095-7882

Abstract: It is essential to elucidate the shear mechanical behavior of structural planes to assess the risk to rock masses and protect them from shear failure. Current research on shear mechanical behavior is focused on isotropic structural planes with the same lithology on both sides. However, anisotropic structural planes, commonly found in nature, may exhibit unique mechanical behavior that differs from isotropic structural planes. Therefore, it is necessary to study the factors affecting the shear strength of the anisotropic structural planes. In this paper, the direct shear numerical tests on anisotropic structural planes were carried out using the three-dimensional distinct element code (3DEC) based on the laboratory test. The numerical test results illustrate that the error between the peak shear strength of the numerical test and the laboratory test is basically within 10%. The shear stress-displacement curves of the numerical and laboratory tests are similar, which verifies the accuracy of the numerical test. According to the Barton standard sections, anisotropic structural plane models with different roughness and size were established, and the direct shear numerical tests with different normal stresses were carried out. To predict the peak shear strength of the anisotropic structural planes, one hundred and eighty-one sets of direct shear numerical test data were selected. Normal stress, roughness, compressive strength of soft and hard rock masses, basic friction angle of soft and hard rock masses, and structural plane size were used as input parameters to establish a back propagation (BP) neural network model. The research results show that, under identical conditions, the shear strength of the anisotropic structural planes decreases as the structural plane size increases. On the contrary, the shear strength increases with the increasing structural plane roughness and normal stress. For the BP neural network prediction model, the root mean square error (RMSE) and coefficient of determination (R^2) of the training set are 0.441 and 0.957. For the test set, the RMSE is 0.489, and R^2 is 0.947, which indicates that the predicted values are in good agreement with the actual values.

Keywords: anisotropic structural plane; shear strength; discrete element method; size effect; neural network

Academic Editor: José António Correia

Received: 24 December 2024
Revised: 8 January 2025
Accepted: 24 January 2025
Published: 3 February 2025

Citation: Ma, W.-B.; Zou, W.-H.; Zhang, J.-L.; Li, G. Prediction of Shear Strength in Anisotropic Structural Planes Considering Size Effects. *Designs* **2025**, *9*, 17. https://doi.org/10.3390/designs9010017

1. Introduction

Structural planes are specialized surfaces formed within rock masses during geological evolution. These features typically exhibit low shear strength, making them the weakest zones within the rock mass. As a result, the structural plane plays a critical role in influencing the stability of rock slopes and tunnels [1–4]. Scientists have indicated that the thickness,

joint roughness coefficient (JRC), and basic friction angle of the structural plane have a great influence on the shear mechanical behaviors contributing to the instability of rock slope [5–8]. There were numerous documented cases of engineering failures attributed to insufficient structural plane strength. In 2019, a significant landslide occurred in Shuicheng County, China. Investigations revealed that weak structural planes were one of the main causes of rainfall-induced landslides [9]. Additionally, in 2021, a large landslide took place in Tiejiangwan, where the failure was also linked to the presence of weak structural planes [10]. In 2022, the Luding earthquake in China triggered landslides in accumulated deposits. The primary cause was the presence of numerous discontinuities in the hard rock regions, which were prone to sliding along discontinuities and fracturing under seismic loading, leading to rock mass instability [11].

Numerous scholars have conducted in-depth studies on the factors influencing the shear strength of rock mass structural planes, with structural plane roughness being recognized as a critical determinant. Natural structural planes are typically structurally complex and have irregular surface undulations. Their roughness exhibits significant size effect as well as heterogeneity and anisotropy, posing substantial challenges for the accurate description and quantitative analysis of their mechanical behavior [12,13]. Over the past 50 years, scholars have proposed various methods to quantify the roughness of rock mass structural planes, including statistical parameters, fractal theory, and 3D scanning techniques. Barton [14], through experimental studies, derived an empirical formula for the peak shear strength of rock mass structural planes, and the joint roughness coefficient (JRC) was introduced. Due to the simplicity of JRC, it has been widely adopted for evaluating the mechanical properties of structural planes [15]. Barton et al. [16] proposed a nonlinear criterion for the shear strength of rock mass structural planes and subsequently refined its shear strength component. This improvement incorporated new parameters, such as JCS (Joint Compressive Strength), providing significant enhancements to account for the scale effect within the criterion. In addition, the visual comparison method was proposed for estimating the JRC values of structural planes. By characterizing 136 natural structural planes from seven different rock types, they ultimately selected 10 representative structural planes as typical examples. In 1978, the visual comparison method was adopted as the standard approach for evaluating the roughness of structural planes by the International Society for Rock Mechanics. However, this method heavily relies on the subjective judgment of the evaluator, leading to significant errors. To reduce these errors and improve the accuracy of JRC assessments, scholars have proposed various modifications to the visual comparison method. Considering that undulation amplitude and frequency are two critical parameters influencing roughness, Ünlüsoy et al. [17] proposed evaluating JRC values by measuring the similarity between the surface profile of samples and the Barton standard sections in the spatial frequency domain, using a third-order polynomial function and power spectral density. To address the challenge of estimating the roughness of longer structural planes using Barton standard sections, Barton and Bandis [18] introduced the straightedge method for determining JRC values. Du et al. [19] rigorously reformulated the Barton straightedge method, proposing a simplified formula more suitable for field measurements. Considering the fractal dimension and magnitude distribution of the asperities, Stigsson et al. [20] developed a multilinear model developed to estimate JRC objectively.

In recent years, scholars have carried out numerous laboratory experiments on the shear strength of rock mass structural planes. Failure characteristics of structural planes were studied under various loading conditions and structural plane parameters. Wang et al. [21] studied the relationship between the shear mechanical properties of structural planes and acoustic emission parameters under different roughness and anchorage conditions, revealing four stages of the ideal cumulative influence curve during the shear

of the structural plane. It is found that the models with 0–60 degree inclination direction had poor stability. Feng et al. [22] conducted shear tests with varying roughness and normal stress, revealing how mechanical properties change due to these two factors. The relationship equations with normal stress and roughness were established for various mechanical parameters. Meng et al. [23] conducted shear tests on completely occlusive granite structural planes formed by tensile splitting under various normal stresses and monitored the acoustic emission during the shear process. The stress drop caused by the uneven surface of the granite rigid structure plane was reproduced, and a method to predict stress drop and fault sliding rock burst was established based on the acoustic emission b value. Du et al. [24] developed a shear strength size effect direct shear testing system for the structural planes, analyzing the influence of size effect on the ratio of the tangential load peak value to the normal load. According to the Coulomb-Navier criterion, Mashhadiali et al. [25] proposed a theoretical model for predicting the shear strength of anisotropic rocks, in which failure depends on the inclination of inherent structural weak planes. The shear sliding tests under unloading normal stress regarding various initial normal stresses and numbers of shearing cycles were conducted by Yin et al. [26], illustrating how JRC, normal stress, and numbers of shearing cycles affected the shear behavior of structural planes.

However, as the primary method for obtaining the shear strength of rock mass structural planes, laboratory direct shear tests still have limitations. These tests struggle to fully replicate the original stress conditions of rock samples and cannot accurately reproduce the complex geometries of natural rock mass structural planes. Furthermore, large-scale laboratory direct shear tests are time-consuming and labor-intensive. While full-scale in situ tests can avoid sampling challenges and maintain the original state of specimens, they involve complex and hazardous testing environments, difficult equipment operations, and significantly higher costs. In recent years, the rapid advancement of information and computer technologies has increased reliance on simulation software for mechanical numerical tests [27–30]. Additionally, machine learning algorithms are being increasingly applied to analyze experimental data [31–35]. These methods, which have gained widespread recognition in the academic community, help to overcome the time and cost constraints associated with traditional laboratory experiments. Based on the physical and numerical modeling, Menhendra et. al found a new geological phenomenon that there is an important relationship between the direction of the joint and the lateral strain ratio [36]. The failure modes of shallow-buried long-span tunnels were analyzed by Chen et al. [37] using the universal distinct element code. Their study revealed that weak structural planes are the primary cause of shear failure in the overlying strata, which ultimately leads to the occurrence of staggered traction slip collapses. Using particle flow code, Yuan et al. [38] established the correlation between the failure mode of the structural plane and the intensity of energy release, finding that the AE b-value can be used to predict the shear failure of the rock structural plane. Numerical tests of anisotropic deformation around a tunnel were conducted by Wang and Huang [39]. The results show that when a rock mass contains two sets of structural planes with unfavorable orientations, the regions experiencing structural plane sliding failure can exacerbate each other, leading to significant anisotropic deformation. To avoid stress concentration when using PFC2D to simulate the shear behavior of the rock mass structural plane, Guo et al. [40] proposed the method of particle group contact discrimination on both sides of the structural plane.

In natural rock masses, anisotropic structural planes with significantly different lithology on both sides are widely distributed, in addition to isotropic structural planes. However, the current research on the shear strength of rock mass structural planes mainly focuses on isotropic structural planes, while the research on anisotropic structural planes is relatively

small. Especially when considering the size effect, the systematic research on the shear strength of anisotropic structural planes is still insufficient, which limits the understanding and effective prediction of the shear behavior of structural planes in complex rock mass engineering. Hence, based on 3DEC and the backpropagation (BP) neural network model, the size effect of the shear strength of rock structural planes was studied. Taking the roughness, size, and normal stress as the variables, direct shear numerical tests of anisotropic structural planes were carried out. The shear characteristics of anisotropic structural planes were studied. The peak shear strength was predicted and analyzed. The research results can provide a scientific reference for predicting the mechanical behavior of structural planes in complex rock mass engineering.

2. The 3DEC Models for Shear Testing of Anisotropic Structural Planes

2.1. Overview of 3DEC

The 3DEC is based on the discrete element method to describe the mechanical behavior of discrete media. It inherits the basic core idea of UDEC and is essentially the result of extending the description of the two-dimensional discrete media mechanics to three-dimensional space. The 3DEC is widely recognized for its ability to model the mechanical interactions of discrete blocks. Considering not only the deformability of individual blocks but also the complex mechanical behavior of joints, the structural response under various loading conditions can be studied in detail by the 3DEC. Therefore, 3DEC is used to analyze the role of joints, faults, and fractures in the overall response of rock mass.

2.2. Model Establishment and Grid Division

A flat structural plane and two Barton standard sections, whose JRC were 0, 2.8, and 10.8, were selected as the anisotropic structural plane models. According to JRC, from small to large, these structural planes were numbered R1, R2, and R3. Their morphologies are shown in Figure 1.

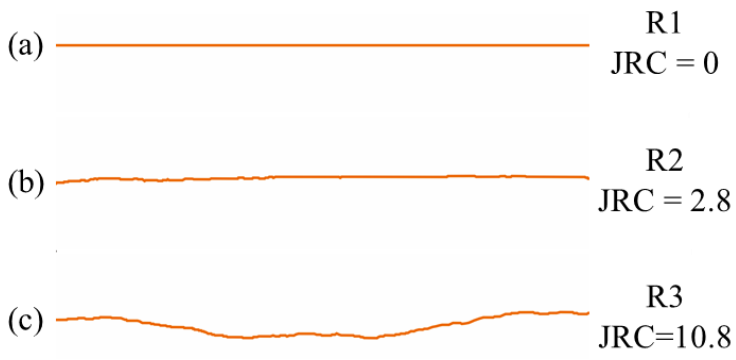

Figure 1. Morphologies of structural plane: (**a**) R1; (**b**) R2; (**c**) R3.

The structural plane section line was drawn in the CAD drawing software; the model was exported in the STL format and imported into the Rhino software. A 10 cm × 10 cm × 10 cm block of the same size as the direct shear laboratory test was created in Rhino. The boolean operation separation command divided the cubic block into two identical rectangular blocks using the structural plane section line. The structural plane models were meshed with an element size of 5 mm, and the unstructured tetrahedral elements were created in the Griddle. The established Rhino models were imported into the 3DEC software in the 3dgrid format for modeling. The established models are shown in Figure 2.

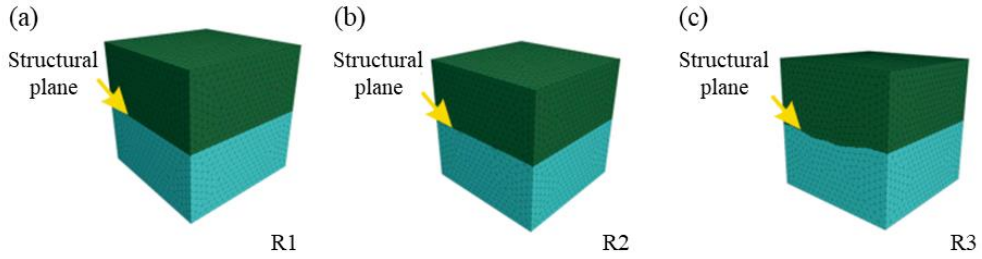

Figure 2. Numerical model of anisotropic structural planes with different roughnesses: (**a**) R1; (**b**) R2; (**c**) R3.

2.3. Material Assignment and Boundary Condition Setting

Sandstone, granite, and cement mortar were used as direct shear laboratory test materials. The cement mortar samples were prepared by mixing cement, sand, and water. The materials mentioned above were assumed to be uniform, with no apparent discontinuities or defects. The basic mechanical parameters of the three materials were obtained through laboratory tests, as shown in Table 1.

Table 1. Basic mechanical parameters of sandstone, granite, and cemented mortar rock samples.

Materials	Density (g/cm^3)	Elasticity Modulus (GPa)	Bulk Modulus (GPa)	Shear Modulus (GPa)	Cohesion (MPa)	Basic Friction Angle (°)	Tensile Strength (MPa)	Compressive Strength (MPa)
Sandstone	2.42	18.85	10.47	7.86	3.07	29.60	2.13	95.55
Granite	2.81	57.92	38.61	23.17	10.33	35.00	6.47	261.55
Cement mortar	2.11	22.33	12.41	9.30	5.03	31.50	1.81	32.61

In the numerical test, the Mohr-Coulomb model was used for the block, and the Coulomb slip joint model was used for the structural plane. To verify the accuracy of the numerical test, the normal stress and shear rate were consistent with those in the laboratory test. During the numerical test, four normal stress levels were applied, namely, 0.5 MPa, 1 MPa, 2 MPa, and 3 MPa. The normal stress was maintained constant throughout the single shearing process, while a tangential load was applied to control the shear rate at 0.5 mm/min. The boundary conditions of the models are shown in Figure 3.

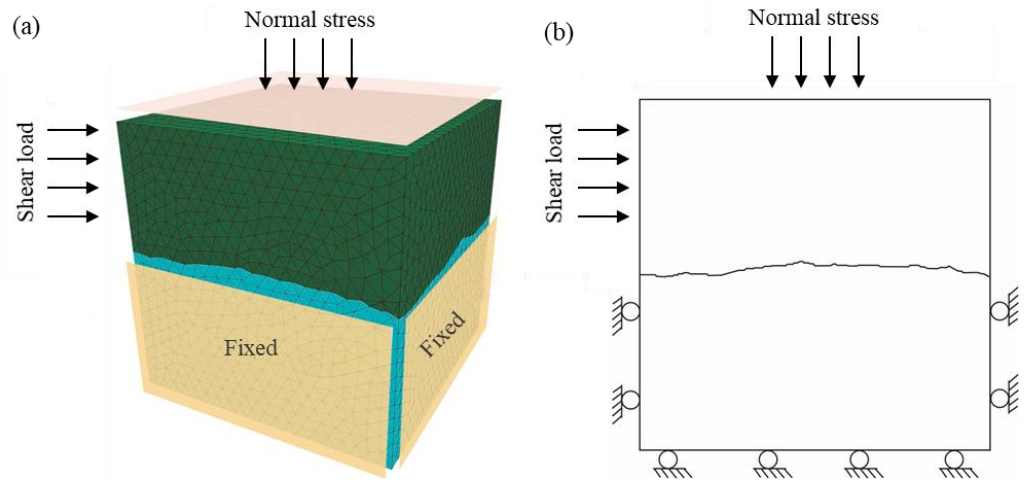

Figure 3. Boundary conditions of the established model: (**a**) Three-dimensional boundary conditions; (**b**) Two-dimensional boundary conditions.

2.4. Analysis and Accuracy Verification of Numerical Results of the Direct Shear Test on the Anisotropic Structural Plane

The shear strength data of the anisotropic structural planes used for accuracy verification are taken from the direct shear laboratory test of rock–mortar anisotropic structural planes conducted by Zhou [41]. The results of the direct shear numerical tests on the structural plane are further derived and compared with the shear strength obtained from the laboratory test. The shear displacement–stress curves of the structural planes with different roughness conditions are given in Figures 4 and 5.

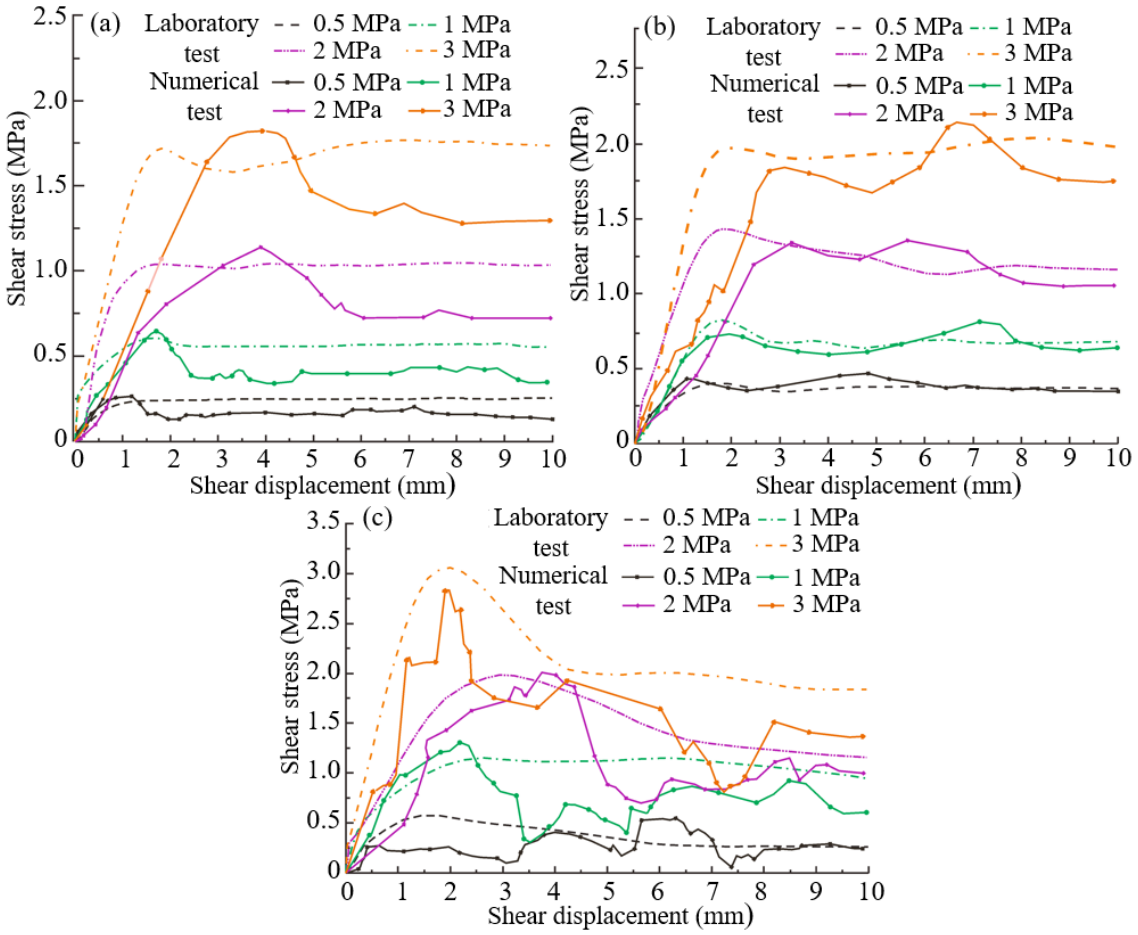

Figure 4. The relationship between shear stress and shear displacement of sandstone-mortar structural planes: (**a**) R1; (**b**) R2; (**c**) R3.

By assessing the shear displacement–stress curve of the anisotropic structural plane, it is found that the shear displacement–stress curve of the anisotropic structural plane can be roughly divided into an ascending stage, a descending stage, and a stable stage. The numerical results show roughly the same trend as the shear displacement–stress curve obtained from the laboratory test. Under the same normal stress conditions, the fluctuation amplitude of the structural plane morphology has a significant effect on the shear behavior. When the fluctuation amplitude of the structural plane morphology is low, the roughness is relatively small and does not contribute significantly to shear resistance. As a result, the fluctuation of the shear displacement–stress curve of the structural plane is small, entering a relatively stable softening deformation stage. The shear strength of the structural plane is close to its residual strength. On the contrary, when the fluctuation amplitude of the structural plane is high, the pronounced roughness creates significant interlocking effects during shearing. These roughness features resist displacement, causing abrupt stress redistributions and localized failures as they deform or break. This mechanism results

in multiple stress peaks on the shear displacement–stress curve, indicating intermittent asperity failure and re-engagement, making it difficult to identify the residual strength value of the structural plane. Table 2 shows the comparison results of the peak shear strength of the anisotropic structural plane with different roughnesses and normal stress conditions. The error, which is basically stable within 10%, between the numerical results and the test results is small.

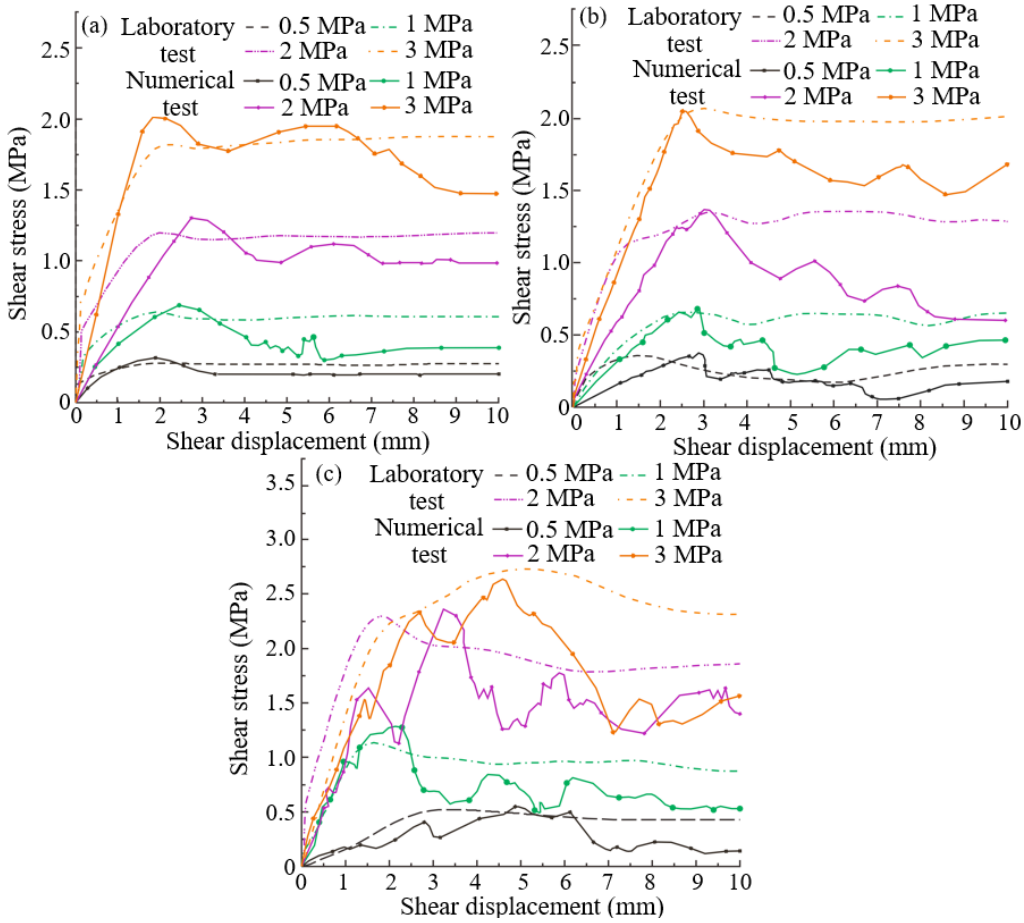

Figure 5. The relationship between shear stress and shear displacement of granite-mortar structural planes: (**a**) R1; (**b**) R2; (**c**) R3.

Table 2. Comparison between laboratory test and numerical test for peak shear strength of anisotropic structural planes.

Anisotropic Structural Plane Types	JRC	Normal Stress (MPa)	Peak Shear Strength (MPa)		Error (%)
			Laboratory Test	Numerical Test	
Sandstone-Cement	R1(JRC = 0)	0.5	0.26	0.26	2.48
		1.0	0.61	0.65	6.01
		2.0	1.05	1.14	8.40
		3.0	1.77	1.89	6.23
	R2(JRC = 2.8)	0.5	0.41	0.45	10.30
		1.0	0.82	0.82	0.19
		2.0	1.43	1.38	3.60
		3.0	2.04	2.20	7.60
	R3(JRC = 10.8)	0.5	0.58	0.55	5.50
		1.0	1.15	1.30	12.80
		2.0	1.99	2.01	1.30
		3.0	3.06	2.84	7.30

Table 2. *Cont.*

Anisotropic Structural Plane Types	JRC	Normal Stress (MPa)	Peak Shear Strength (MPa)		Error (%)
			Laboratory Test	Numerical Test	
Granite-Cement	R1(JRC = 0)	0.5	0.29	0.31	9.10
		1.0	0.64	0.68	6.50
		2.0	1.20	1.30	8.10
		3.0	1.88	2.07	10.50
	R2(JRC = 2.8)	0.5	0.36	0.37	3.70
		1.0	0.66	0.68	2.90
		2.0	1.35	1.35	0.17
		3.0	2.07	2.06	0.54
	R3(JRC = 10.8)	0.5	0.52	0.55	5.90
		1.0	1.13	1.27	12.30
		2.0	2.29	2.37	3.40
		3.0	2.73	2.62	4.10

3. Numerical Shear Testing of Anisotropic Structural Planes with Size Effect

3.1. Design of Direct Shear Numerical Test

The 3rd, 5th, 8th, and 10th sections of Barton standard sections, which were numbered B1 to B4 from small to large according to JRC, were selected. The Rhino modeling software was used to establish the numerical models of the structural planes based on B1 to B4. The rock masses in the upper and lower plates were given strength parameters of different sizes to establish the anisotropic structural plane. The anisotropic structural plane models are shown in Figure 6.

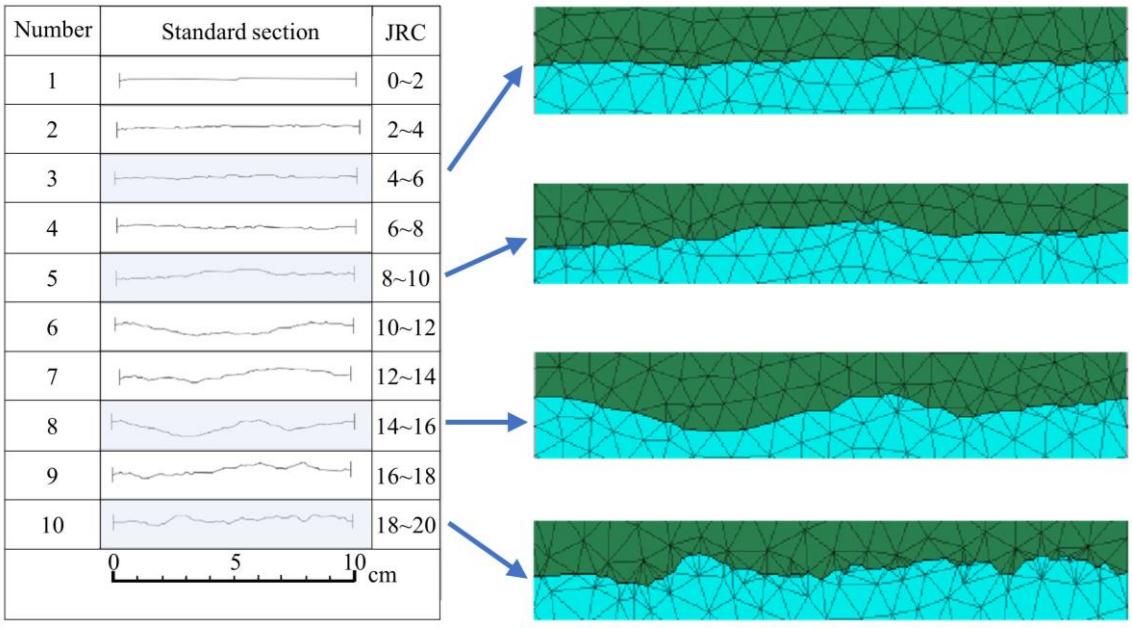

Figure 6. B1–B4 structural plane topography.

To investigate the effects of normal stress, roughness, and size on the peak shear strength of anisotropic structural planes, numerical models of various structural plane roughness were developed with the following dimensions: 10 cm × 10 cm; 30 cm × 30 cm; 50 cm × 50 cm; 70 cm × 70 cm; and 100 cm × 100 cm. Normal stresses of 0.5 MPa, 1 MPa, 2 MPa, 3 MPa, and 5 MPa were applied to the structural planes of each model incrementally. The typical shear displacement–stress curve of the anisotropic structural plane obtained

from the experiment is shown in Figure 7. The shear process of the structural plane could be divided into three stages: elastic; failure; and residual. In the elastic stage, the shear stress is proportional to the shear displacement. In the failure stage, brittle failure occurs inside the rock mass, whose shear strength reaches a peak value, with the shear stress value fluctuating greatly. During the residual stage, the shear stress drops sharply to the residual strength, tending to stabilize and remain constant.

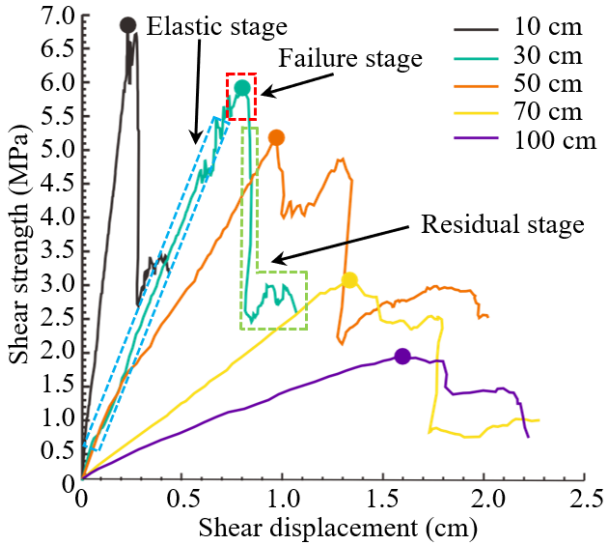

Figure 7. The relationship between shear strength and shear displacement of B1 structural plane with normal stress of 5 MPa.

3.2. Size Effect on Peak Shear Strength of Anisotropic Structural Planes

The size effect of the structural plane has an important influence on the strength and deformation capacity of the rock mass. Figure 8 demonstrates the relationship between the peak shear strength and the size of the anisotropic structural plane. The peak shear strength of all four structural planes (B1 to B4) decreases with increasing size, demonstrating a clear size effect on peak shear strength. Comparing the peak shear strength of the rock mass structural planes from B1 to B4, it can be seen that, for the same normal stress, the peak shear strength is negatively correlated with the size of the structural plane. Under the normal stress of 0.5 MPa, the peak shear strength of the B1 structural plane decreases by 0.022 MPa per 1 cm increase in size. When the normal stress is increased to 5 MPa, the peak shear strength decreases by 0.045 MPa for each 1 cm size increment. Under the normal stress of 0.5 MPa, the peak shear strength of the B2 structural plane decreases by 0.025 MPa per 1 cm increase in size. When the normal stress is increased to 5 MPa, the peak shear strength decreases by 0.053 MPa for each 1 cm size increment. Under the normal stress of 0.5 MPa, the peak shear strength of the B3 structural plane decreases by 0.027 MPa per 1 cm increase in size. When the normal stress is increased to 5 MPa, the peak shear strength decreases by 0.053 MPa for each 1 cm size increment. Under the normal stress of 0.5 MPa, the peak shear strength of the B4 structural plane decreases by 0.031 MPa per 1 cm increase in size. When the normal stress is increased to 5 MPa, the peak shear strength decreases by 0.066 MPa for each 1 cm size increment. The peak shear strength of structural planes decreases slowly with increasing size under low normal stress, while the downward trend increases under high normal stress.

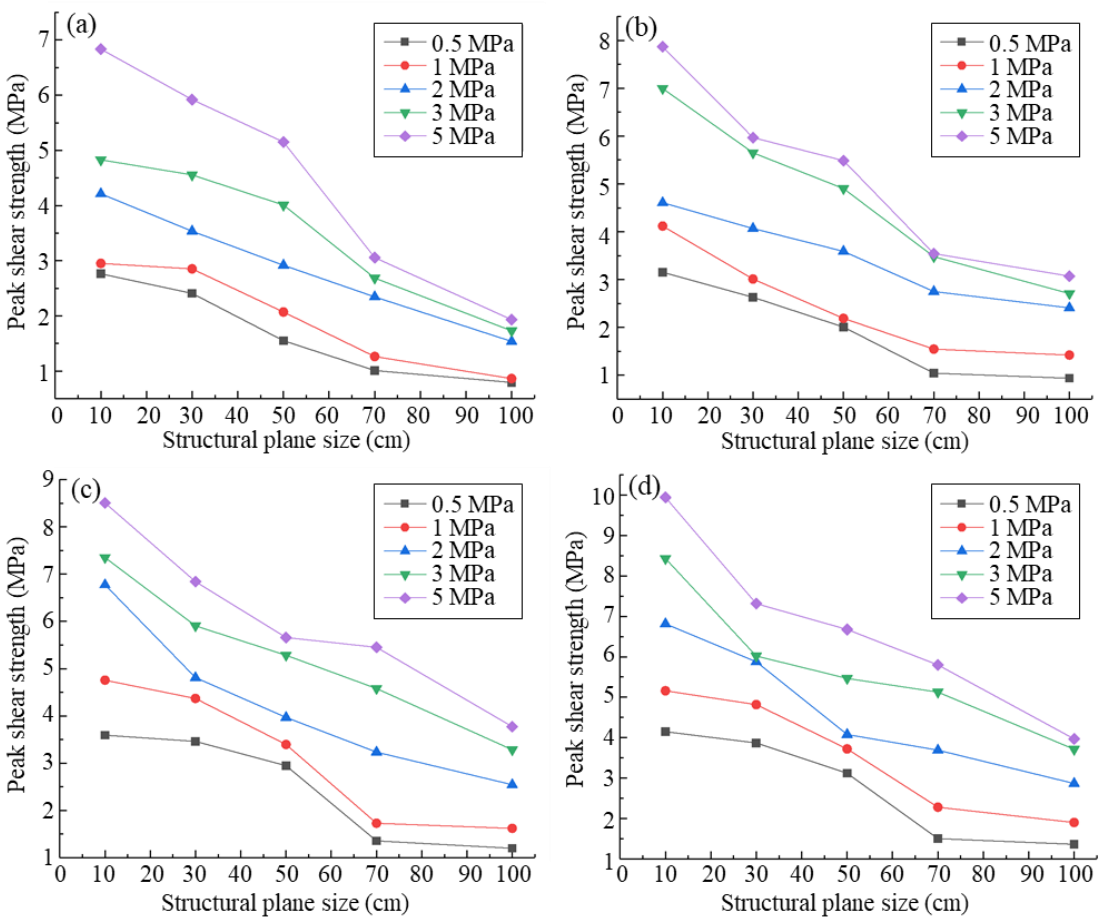

Figure 8. The relationship between peak shear strength and size of the anisotropic structural planes with different roughnesses: (**a**) B1; (**b**) B2; (**c**) B3; (**d**) B4.

3.3. Effect of Normal Stress on Peak Shear Strength of Anisotropic Structural Planes

In the direct shear test, the normal stress also has an important influence on the shear strength of the rock mass structural plane. Figure 9 shows the relationship between the peak shear strength and normal stress of the anisotropic structural plane. The peak shear strength of an anisotropic structural plane increases with higher normal stress for the same size. For the B1 structural plane, when its size is 10 cm, the peak shear strength increases by 0.904 MPa for every 1 MPa increase in normal stress. When the structural plane size reaches 100 cm, the peak shear strength increases by 0.253 MPa per 1 MPa rise in normal stress. For the B2 structural plane, when its size is 10 cm, the peak shear strength increases by 1.049 MPa for every 1 MPa increase in normal stress. When the structural plane size reaches 100 cm, the peak shear strength increases by 0.473 MPa per 1 MPa rise in normal stress. For the B3 structural plane, when its size is 10 cm, the peak shear strength increases by 1.093 MPa for every 1 MPa increase in normal stress. When the structural plane size reaches 100 cm, the peak shear strength increases by 0.571 MPa per 1 MPa rise in normal stress. For the B4 structural plane, when its size is 10 cm, the peak shear strength increases by 1.287 MPa for every 1 MPa increase in normal stress. When the structural plane size reaches 100 cm, the peak shear strength increases by 0.580 MPa per 1 MPa rise in normal stress. At low normal stress, the peak shear strength of structural planes of different sizes tends to be similar. However, as normal stress rises, the differences in peak shear strength become more pronounced, indicating that normal stress significantly influences the peak shear strength of the structural plane.

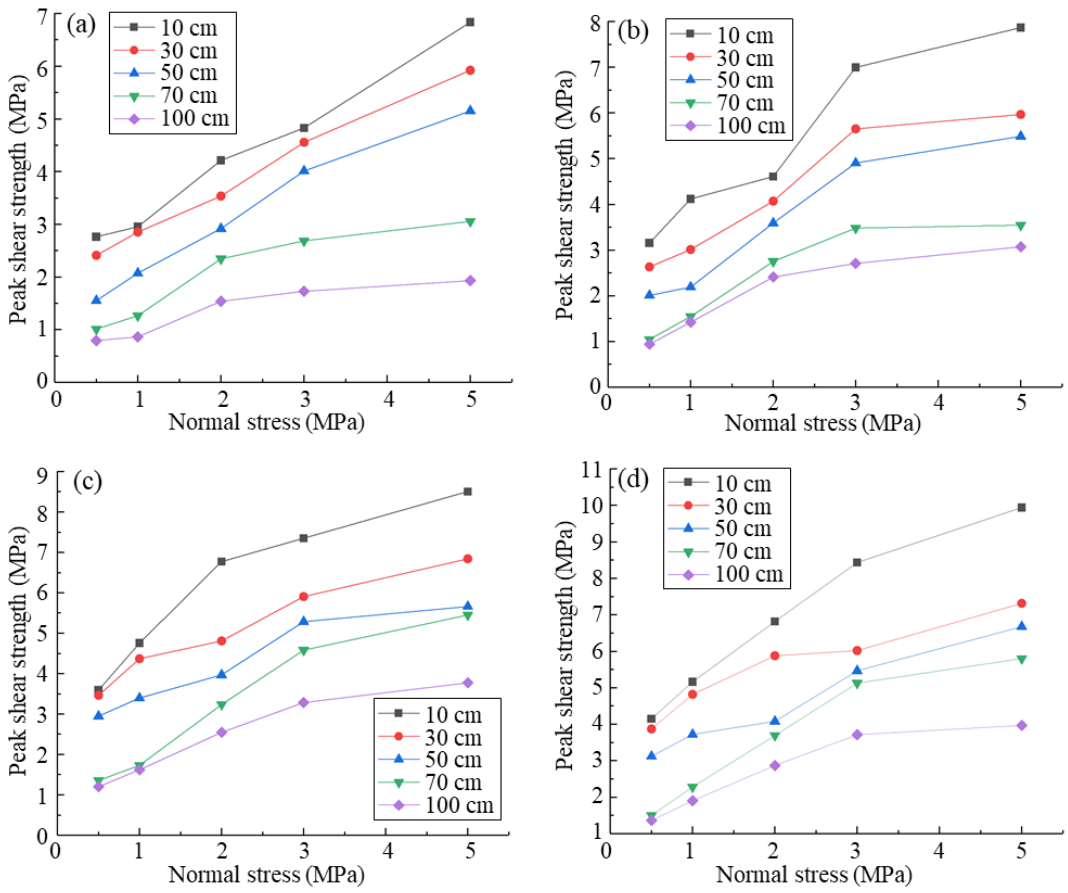

Figure 9. The relationship between peak shear strength and normal stress of the anisotropic structural planes with different roughnesses: (**a**) B1; (**b**) B2; (**c**) B3; (**d**) B4.

3.4. Effect of Roughness on Peak Shear Strength of Anisotropic Structural Planes

The roughness of the structural plane of the rock mass is an important component for its shear strength, especially in the presence of filled joints, where the roughness of the structural plane can lead to an increase in expansibility, local stress, and permeability [42,43]. Table 3 shows the peak shear strength calculated by numerical tests of anisotropic structural planes with different sizes. Under the same normal stress, the peak shear strength of the structural plane increases with the increasing roughness. The tooth-cutting effect is enhanced because the increasing roughness reduces the climbing and expansion effect of the structural plane. In addition, the peak shear strength of the structural plane decreases with increasing size because smaller blocks have greater degrees of freedom and can perceive larger fluctuations in the structural plane. Hence, the roughness decreases when the size increases, which reduces the peak shear strength.

Table 3. Peak shear strength values of anisotropic structural planes with different roughnesses.

Size (cm)	Roughness	Normal Stress (MPa)				
		0.5	1	2	3	5
10	B1	2.76	2.95	4.21	4.83	6.83
	B2	3.15	4.12	4.61	6.99	7.87
	B3	3.59	4.76	6.77	7.35	8.51
	B4	4.15	5.16	6.81	8.43	9.94
30	B1	2.41	2.85	3.53	4.55	5.92
	B2	2.63	3.01	4.07	5.65	5.97
	B3	3.46	4.37	4.81	5.90	6.84
	B4	3.87	4.82	5.86	6.02	7.31

Table 3. *Cont.*

Size (cm)	Roughness	Normal Stress (MPa)				
		0.5	**1**	**2**	**3**	**5**
50	B1	1.55	2.07	2.92	4.01	5.15
	B2	2.01	2.19	3.59	4.90	5.49
	B3	2.95	3.40	3.97	5.28	5.66
	B4	3.12	3.72	4.08	5.47	6.67
70	B1	1.01	1.26	2.34	2.68	3.05
	B2	1.04	1.55	2.75	3.48	3.54
	B3	1.35	1.73	3.23	4.58	5.45
	B4	1.50	2.28	3.69	5.13	5.79
100	B1	0.79	0.86	1.54	1.73	1.93
	B2	0.94	1.42	2.41	2.71	3.07
	B3	1.20	1.62	2.54	3.28	3.77
	B4	1.36	1.90	2.87	3.72	3.97

4. BP Neural Network Model for Predicting Peak Shear Strength of Anisotropic Structural Planes

4.1. Overview of BP Neural Network

A backpropagation neural network is a multi-layer feedforward neural network, including an input layer, a hidden layer, and an output layer. Figure 10 shows a typical three-layer BP neural network structure diagram. The training samples are input into the hidden layer, and after the training function is calculated, the actual output is sent to the output layer. After one propagation, the error between the actual output and the target output is calculated to determine whether it is less than the target error. If the actual error is greater than the target error, the neural network starts to propagate information backward. The actual output is propagated toward the input layer, and neurons in each layer adjust and correct weights and thresholds based on the information received. The neural network will continue to iterate until the calculation result meets the target error. Each connection weight and threshold in the initial training is assigned a random value in the interval (0, 1).

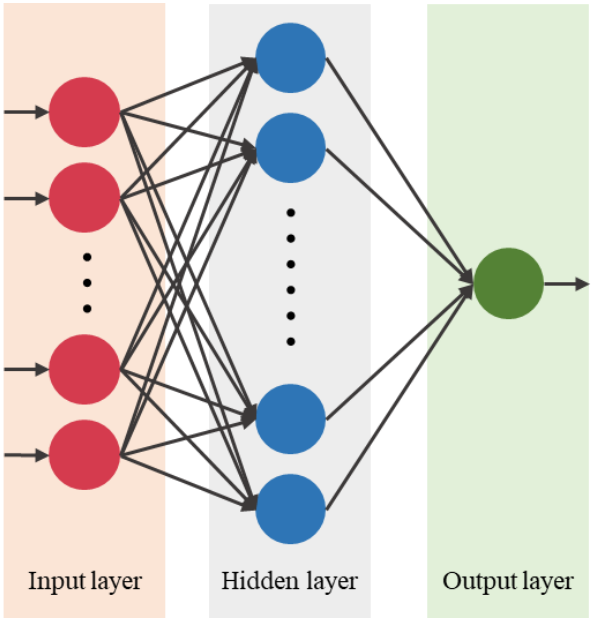

Figure 10. BP neural network structure diagram.

4.2. Design of BP Neural Network

To quantify the JRC value of the Barton standard sections, the morphological analysis method is adopted. The modified straight edge method formula Equations (1) and (2) and the basic roughness scale shown in Figures 11 and 12 are employed to obtain the JRC values of structural planes of different sizes. Table 4 lists the JRC, which is calculated by Equations (1) and (2), of anisotropic structural planes with different roughness.

$$JRC = 0.8589e^{0.6444/L}\arctan 8R_A \quad (1)$$

$$R_A = \frac{A}{L} \quad (2)$$

where A is the height of the larger sawtooth or the fluctuation amplitude of the structural plane, and L is the sampling length of the structural plane.

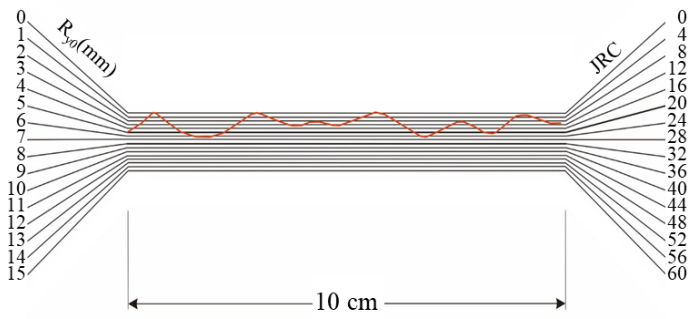

Figure 11. Basic roughness ruler.

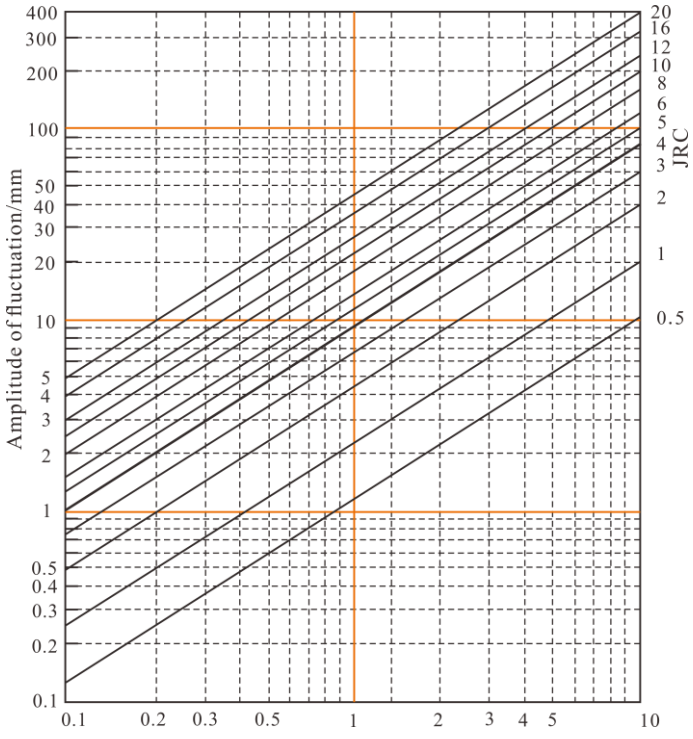

Figure 12. Schematic diagram of the straight edge method for calculating the roughness of structural planes [44].

Table 4. JRC values calculated using the modified straight-edge method.

Number of Structural Planes	Amplitude of Fluctuation	JRC
B1	0.17	0.67
B2	0.65	2.69
B3	1.26	5.24
B4	1.60	6.65
B5	2.27	9.39
B6	2.73	11.25
B7	3.37	13.79
B8	3.88	15.76
B9	4.26	17.21
B10	4.76	19.07

The Barton standard sections proposed by Barton are selected to establish structural planes with different roughness. Eighty-one groups of orthogonal tests are designed using SPSS software. Then, the peak shear strength values of 81 groups of anisotropic structural planes are calculated using 3DEC. The 81 groups of orthogonal test data and 100 groups of test data of B1–B4 structural planes under different sizes and normal stresses are divided into training data and test data according to the proportion imported into the neural network for training. The input parameters of the neural network are normal stress, roughness (JRC), compressive strength of soft and hard rock mass, basic friction angle of soft and hard rock masses, and structural plane size. The output parameter is the peak shear strength of the structural plane. The hidden layer is set to one layer, whose number of units is 11. The neural network training process is shown in Figure 13.

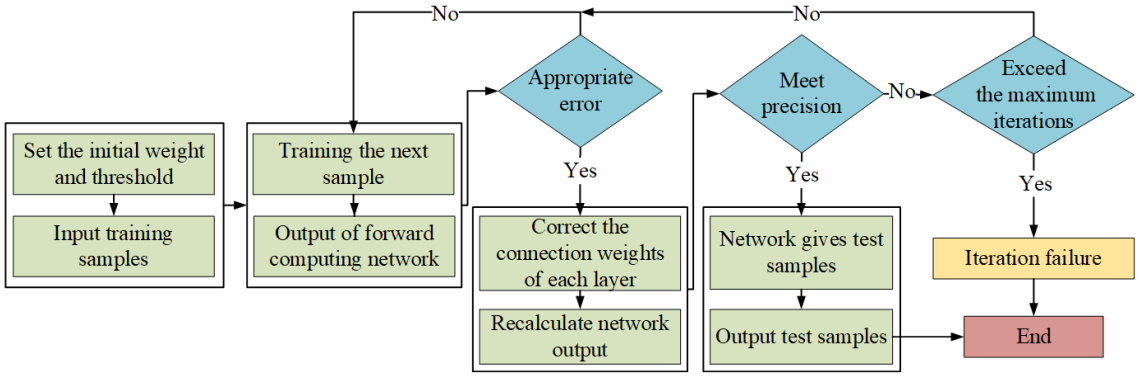

Figure 13. BP neural network training flowchart.

4.3. Prediction Results of Peak Shear Strength

Root mean square error (RMSE) and coefficient of determination (R^2) are used as model performance evaluation indicators [45]. Among them, RMSE is an error evaluation indicator. The closer its value is to 0, the better the model performance. R^2 is a trend evaluation indicator. The closer R^2 is to 1, the closer the model prediction result is to the true value and the higher the prediction accuracy. The calculation formulas Equations (3) and (4) for model evaluation indicators are as follows:

$$RMSE = \sqrt{\frac{1}{N}\sum_{i=1}^{N}\left(m_{\text{exp}} - m_{\text{pred}}\right)^2} \tag{3}$$

$$R^2 = 1 - \frac{\sum_{i=1}^{N}\left(m_{\text{exp}} - m_{\text{pred}}\right)^2}{\sum_{i=1}^{N}\left(m_{\text{exp}} - m_{\text{ea}}\right)^2} \tag{4}$$

where m_{exp} is the actual value; m_{pred} is the predicted value; m_{ea} is the mean of the experimental test value, and N is the number of samples.

To obtain better generalization performance, the optimal number of training times should be determined when the number of hidden layer nodes is fixed. Therefore, the neural network is trained and tested alternately, and a training mean square error is recorded for each iteration. Meanwhile, the network weights should be unchanged, the network should be run forward with the test data, and the test mean square error should be recorded. As a result, two curves can be generated showing the error changing with the number of training times. Before a certain point in training, as the number of training iterations increases, both the training error and the test error decrease simultaneously. Once this point is surpassed, the training error continues to decrease while the test error starts to increase. This specific number of training iterations is considered the optimal amount. The number of steps for programming verification of the BP neural network is set to 6; that is, the network training verification stops after the error increases six consecutive times. It is indicated from Figure 14 that the convergence speed of the BP neural network prediction model is fast, and the optimal number of training steps is 12.

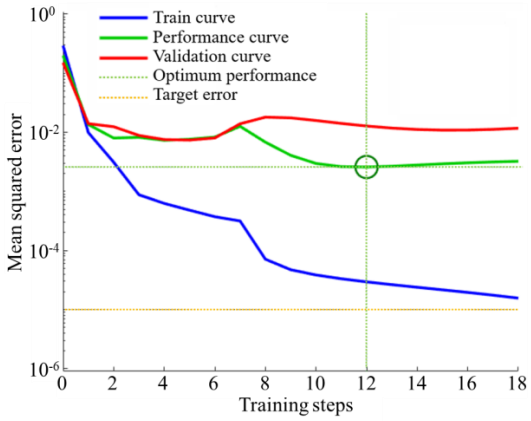

Figure 14. Plot of BP neural network training performance data versus training steps.

Figure 15 compares the actual and predicted values for the peak shear strength of the structural plane in both the training and test sets. The RMSE value of the neural network model is below 0.5 (Figure 15). This indicates a small prediction error, and it shows that the predicted shear strength of the structural plane obtained from the neural network closely aligns with the actual value.

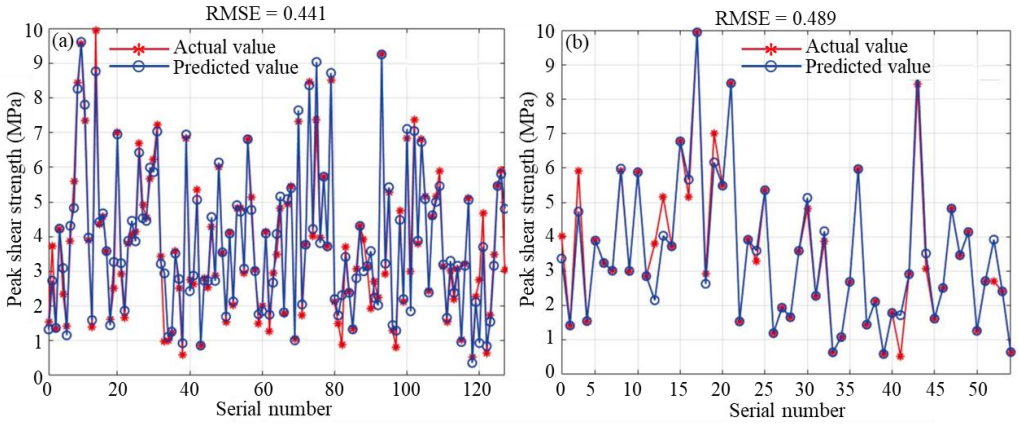

Figure 15. Comparison of actual and predicted values of peak shear strength: (**a**) Training set; (**b**) Test set.

Figure 16 illustrates the linear regression relationship between the actual peak shear strength values of both the training and test samples. The R^2 for the training and test sets are 0.957 and 0.947 (Figure 16), which signifies that the BP neural network model exhibits a strong prediction performance.

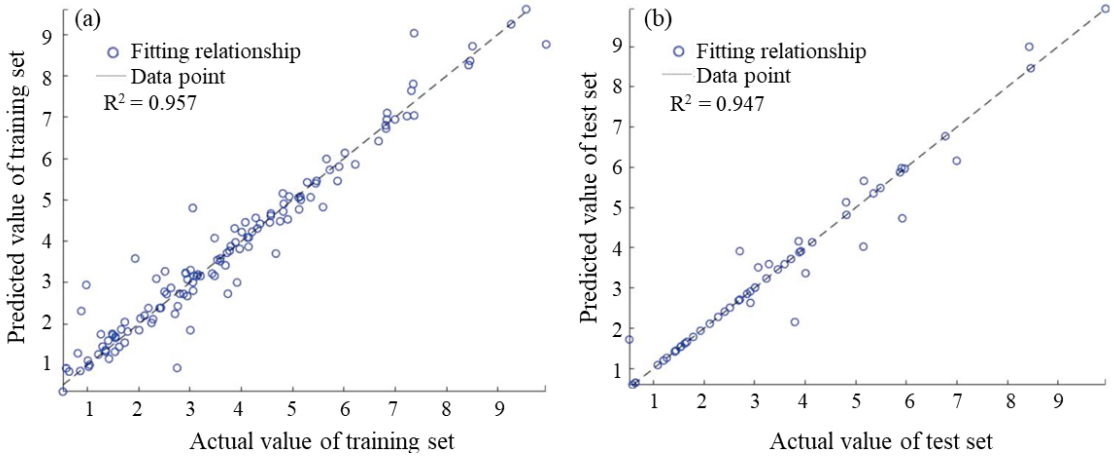

Figure 16. Regression plot between the actual value and the predicted value of the network output: (**a**) Training set; (**b**) Test set.

Combining the results of Figures 15 and 16, it can be seen that the overall regression curve of the predicted value and the actual value shows a high degree of regression, indicating that the predicted value and the actual value of the shear strength of the structural plane are very close. The comparison results indicate that the BP neural network provides a high level of accuracy in predicting the peak shear strength of structural planes. This method can effectively predict the shear strength of anisotropic structural planes.

5. Conclusions

Based on the discrete element method, in this paper, numerical models of anisotropic structural plane were established. After model verification, the direct shear numerical tests of anisotropic structural planes were carried out to evaluate the shear characteristics of structural planes with different sizes, normal stresses, and roughnesses. Then, a BP neural network model for predicting the peak shear strength of the structural plane was developed with numerical test data. The main conclusions are as follows:

(1) A direct shear test model for rock mass with anisotropic structural planes is established using 3DEC. By comparing the numerical and laboratory test results, it has been found that the error in peak shear strength was generally within 10%. Additionally, the shear displacement–stress curve obtained from the numerical tests closely resembles the curve from the laboratory tests, effectively replicating the shear process of the structural plane sample;

(2) The peak shear strength of anisotropic structural planes is negatively correlated with size. When the JRC is 4 to 6, the peak shear strength decreases by 0.022 to 0.045 MPa for every additional 1 cm in size with different normal stresses. When the JRC is from 8 to 10, the peak shear strength decreases by 0.025 to 0.053 MPa for every additional 1 cm in size with different normal stresses. When the JRC is 14 to 16, the peak shear strength decreases by 0.027 to 0.053 MPa for every additional 1 cm in size with different normal stresses. When the JRC is 18 to 20, the peak shear strength decreases by 0.031 to 0.066 MPa for every additional 1 cm in size with different normal stresses;

(3) The peak shear strength of anisotropic structural planes is positively correlated with normal stress and roughness. When the JRC is 4 to 6, the peak shear strength increases

by 0.253 to 0.904 MPa for each 1 MPa increase in normal stress with different sizes. When the JRC is 8 to 10, the peak shear strength increases by 0.473 to 1.049 MPa for each 1 MPa increase in normal stress with different sizes. When the JRC is from 14 to 16, the peak shear strength increases by 0.571 to 1.093 MPa for each 1 MPa increase in normal stress with different sizes. When the JRC is from 18 to 20, the peak shear strength increases by 0.580 to 1.287 MPa for each 1 MPa increase in normal stress with different sizes. Under identical size and normal stress conditions, the shear strength of the large structural plane with a high JRC is consistently the highest;

(4) The optimal number of training steps of the BP neural network model is 12. The RMSE of the BP neural network model is less than 0.5, and the R^2 value is greater than 0.94, which indicates that the predicted results align closely with the actual test results. Therefore, this model can effectively predict the peak shear strength of the anisotropic structural planes within rock masses.

Author Contributions: Conceptualization, W.-B.M. and G.L.; methodology, J.-L.Z. and G.L.; software, W.-B.M. and G.L.; validation, W.-B.M. and G.L.; formal analysis, W.-H.Z. and J.-L.Z.; investigation, W.-H.Z. and G.L.; resources, W.-H.Z.; data curation, W.-B.M.; writing—original draft preparation, W.-B.M.; writing—review and editing, W.-H.Z., J.-L.Z. and G.L.; visualization, W.-H.Z.; supervision, J.-L.Z.; project administration, G.L.; funding acquisition, W.-B.M. and G.L. All authors have read and agreed to the published version of this manuscript.

Funding: This work was supported by the Open Fund of State Key Laboratory of High-speed Railway Track Technology (2022YJ127-1), the National Natural Science Foundation of China (Grant No. 52304092), Zhejiang Provincial Natural Science Foundation (LQ24D020001).

Data Availability Statement: Data are contained within this article.

Acknowledgments: Thanks to the help of anonymous reviewers and journal editors.

Conflicts of Interest: Author Wei-Bin Ma, Wen-Hao Zou, Jin-Long Zhang was employed by the company China Academy of Railway Sciences Corporation Limited. The remaining authors declare that the research was conducted in the absence of any commercial or financial relationships that could be construed as a potential conflict of interest.

References

1. Zhang, L.; Yang, Q.; Liu, Y. Long-term stability analysis of the left bank abutment slope at Jinping I hydropower station. *J. Rock Mech. Geotech.* **2016**, *8*, 398–404. [CrossRef]
2. Zhong, J.H.; Yang, X. Pseudo-dynamic stability of rock slope considering Hoek-Brown strength criterion. *Acta Geotech.* **2022**, *17*, 2481–2494. [CrossRef]
3. Miao, C.; Liu, J.; Gao, M.; Li, J.; Pang, D.; Yuan, K. Insight into the overload failure mechanism of anchored slope with weak structural planes. *Bull. Eng. Geol. Environ.* **2024**, *83*, 390. [CrossRef]
4. Zhang, Z.R.; Wu, S.C.; Cheng, H.Y.; Han, L.; Chang, X.; Fu, X. Experimental study on the influence of structural planes on rockbursts in deep-buried hard-rock tunnels. *Rock Mech. Rock Eng.* **2024**, *57*, 8057–8080. [CrossRef]
5. Vick, L.M.; Böhme, M.; Rouyet, L.; Bergh, S.G.; Corner, G.D.; Lauknes, T.R. Structurally controlled rock slope deformation in Northern Norway. *Landslides* **2020**, *17*, 1745–1776. [CrossRef]
6. Zhao, L.H.; Yu, C.H.; Cheng, X.; Zuo, S.; Jiao, K. A method for seismic stability analysis of jointed rock slopes using Barton-Bandis failure criterion. *Int. J. Rock Mech. Min.* **2020**, *136*, 104487. [CrossRef]
7. Tan, X.; Ren, Y.K.; Li, T.L.; Zhou, S.H.; Zhang, J.C.; Zhou, S.K. In-situ direct shear test and numerical simulation of slate structural planes with thick muddy interlayer along bedding slope. *Int. J. Rock Mech. Min.* **2021**, *143*, 104791. [CrossRef]
8. Deng, D.P. Limit equilibrium analysis on the stability of rock wedges with linear and nonlinear strength criteria. *Int. J. Rock Mech. Min.* **2021**, *148*, 104967. [CrossRef]
9. Zhuang, Y.; Xing, A.; Leng, Y.; Bilal, M.; Zhang, Y.; Jin, K.; He, J. Investigation of characteristics of long runout landslides based on the multi-source data collaboration: A case study of the Shuicheng basalt landslide in Guizhou, China. *Rock Mech. Rock Eng.* **2021**, *54*, 3783–3798. [CrossRef]

10. He, K.; Liu, B.; Hu, X.W.; Zhou, R.; Xi, C.; Ma, G.; Han, M.; Li, Y.; Luo, G. Rapid characterization of landslide-debris flow chains of geologic hazards using multi-method investigation: Case study of the Tiejiangwan LDC. *Rock Mech. Rock Eng.* **2022**, *55*, 5183–5208. [CrossRef]
11. Wu, K.; Yi, X.B.; Fu, X.D.; Zhang, L.; Kang, J.Y.; Yuan, Q.; Shao, J. Geohazard development rules and post disaster reconstruction strategies of Hailuogou scenic road in the epicenter of Luding earthquake. *Chin. J. Rock Mech. Eng.* **2024**, *43*, 1909–1922. (In Chinese)
12. Huang, M.; Luo, Z.Y.; Du, S.G. Experimental study of sampling representativeness of structural plane of rock model. *Chin. J. Rock Mech. Eng.* **2013**, *32*, 2008–2014. (In Chinese)
13. Ming, H.J.; Liu, C.Y.; Wang, Y.X. Numerical simulation of size effect of rock structural plane. *Chin. J. Under Space Eng.* **2016**, *12*, 387–391. (In Chinese)
14. Barton, N. Review of a new shear strength criterion for rock joint. *Eng. Geol.* **1973**, *7*, 287–332. [CrossRef]
15. Tse, R.; Cruden, D.M. Estimating joint roughness coefficients. *Int. J. Rock Mech. Min. Geol. Abs.* **1979**, *16*, 303–307. [CrossRef]
16. Barton, N.; Choubey, V. The shear strength of rock joints in theory and practice. *Rock Mech. Rock Eng.* **1977**, *10*, 1–54. [CrossRef]
17. Ünlüsoy, D.; Süzen, M.L. A new method for automated estimation of joint roughness coefficient for 2D surface profiles using power spectral density. *Int. J. Rock Mech. Min.* **2020**, *125*, 104156. [CrossRef]
18. Barton, N.; Bandis, S. Effects of block size on the shear behavior of jointed rock. In Proceedings of the 23rd US Symposium on Rock Mechanics, Berkeley, CA, USA, 25–27 August 1982; pp. 739–760.
19. Du, X.F.; Du, S.G. Concise formula of Barton's straight edge method for joint roughness coefficient. *J. Eng. Geol.* **2008**, *16*, 196–200. (In Chinese)
20. Stigsson, M.; Ivars, D.M. A novel conceptual approach to objectively determine JRC using fractal dimension and asperity distribution of mapped fracture traces. *Rock Mech. Rock Eng.* **2019**, *52*, 1041–1054. [CrossRef]
21. Wang, G.; Zhang, Y.; Jiang, Y.; Liu, P.; Guo, Y.; Liu, J.; Ma, M.; Wang, K.; Wang, S. Shear behaviour and acoustic emission characteristics of bolted rock joints with different roughnesses. *Rock Mech. Rock Eng.* **2018**, *51*, 1885–1906. [CrossRef]
22. Feng, W.; Zou, D.; Wang, T.; Qiao, C.; Xu, S. Study on a nonlinear shear damage constitutive of structural plane and application of discrete element. *Comput. Geotech.* **2023**, *155*, 105190. [CrossRef]
23. Meng, F.; Zhou, H.; Wang, Z.; Zhang, L.; Kong, L.; Li, S.; Zhang, C. Experimental study on the prediction of rockburst hazards induced by dynamic structural plane shearing in deeply buried hard rock tunnels. *Int. J. Rock Mech. Min.* **2016**, *86*, 210–223. [CrossRef]
24. Du, S.G.; Lyu, Y.J.; Luo, Z.Y.; Huang, M. Combined test system for size effect of rock joint shear strength and its primary application research. *Chin. J. Rock Mech. Eng.* **2021**, *40*, 1337–1349. (In Chinese)
25. Mashhadiali, N.; Molaei, F. Theoretical and experimental investigation of a shear failure model for anisotropic rocks using direct shear test. *Int. J. Rock Mech. Min.* **2023**, *170*, 105561. [CrossRef]
26. Yin, Q.; Zhu, C.; Wu, J.; Pu, H.; Wang, Q.; Zhang, Y.; Jing, H.; Deng, T. Shear sliding of rough-walled fracture surfaces under unloading normal stress. *J. Rock Mech. Geotech.* **2023**, *15*, 2658–2675. [CrossRef]
27. Cao, X.; Wu, M.; Liu, S.; Fang, L.; Wang, B. Deformation simulation of steep over-dip stratified surrounding rock for small angle between tunnel and rock strike. *J. Mt. Sci. Eng.* **2013**, *31*, 385–390.
28. Yin, D.W.; Chen, S.J.; Chen, B.; Liu, X. Strength and failure characteristics of the rock-coal combined body with single joint in coal. *Geomech. Eng.* **2018**, *15*, 1113–1124. [CrossRef]
29. Le, H.L.; Wei, J.H.; Sun, S.R.; Zhang, C.C. Cracking behaviors and strength of rock-like samples with steps of different geometries under shear stress. *J. Mt. Sci. Eng.* **2021**, *18*, 1352–1370. [CrossRef]
30. Renaud, S.; Bouaanani, N.; Miquel, B. Experimental, analytical, and finite element assessment of the shear strength of concrete-rock interfaces at different scales. *Int. J. Numer. Anal. Met.* **2021**, *45*, 1238–1259. [CrossRef]
31. Greco, D.O.; Ferrero, A.M.; Oggeri, C. Experimental and analytical interpretation of the behaviour of laboratory tests on composite specimens. *Int. J. Rock Mech. Min.* **1993**, *30*, 1539–1543. [CrossRef]
32. Ban, L.R.; Zhu, C.; Hou, Y.H.; Du, W.S.; Qi, C.Z.; Lu, C.S. A method to predict the peak shear strength of rock joints based on machine learning. *J. Mt. Sci. Eng.* **2023**, *20*, 3718–3731. [CrossRef]
33. Xu, Z.H.; Guo, G.; Sun, Q.C.; Wang, Q.; Zhang, G.D.; Ye, R.Q. Structural plane recognition from three-dimensional laser scanning points using an improved region-growing algorithm based on the robust randomized Hough transform. *J. Mt. Sci. Eng.* **2023**, *20*, 3376–3391. [CrossRef]
34. Zhou, S.; Lei, Y.; Zhang, Z.-X.; Luo, X.; Aladejare, A.; Ozoji, T. Estimating dynamic compressive strength of rock subjected to freeze-thaw weathering by data-driven models and non-destructive rock properties. *Nondestruct. Test. Eva.* **2024**, *40*, 116–139. [CrossRef]
35. Zhou, S.; Zhang, Z.-X.; Luo, X.; Huang, Y.; Yu, Z.; Yang, X. Predicting dynamic compressive strength of frozen-thawed rocks by characteristic impedance and data-driven methods. *J. Rock Mech. Geotech.* **2024**, *16*, 2591–2606. [CrossRef]

36. Mahendra, S.; Bhawani, S. Laboratory and Numerical Modelling of a Jointed Rock Mass. In Proceedings of the 12th International Conference of International Association for Computer Methods and Advances in Geomechanics (IACMAG), Goa, India, 1–6 October 2008; ISBN 978-162276176-0.
37. Chen, S.; Qiao, C.S.; Yang, Z.; Qiao, C. Application of stochastic joint network simulation to composite strata of shallow-buried long-span metro tunnels. *Bull. Eng. Geol. Environ.* **2020**, *79*, 2085–2107. [CrossRef]
38. Yuan, W.; Cheng, Y.; Min, M.; Wang, X. Study on acoustic emission characteristics during shear deformation of rock structural planes based on particle flow code. *Comput. Part Mech.* **2024**, *11*, 105–118. [CrossRef]
39. Wang, T.T.; Huang, T.H. Anisotropic deformation of a circular tunnel excavated in a rock mass containing sets of ubiquitous Joints: Theory analysis and numerical modeling. *Rock Mech. Rock Eng.* **2014**, *47*, 643–657. [CrossRef]
40. Guo, W.; Zhang, C.; Wang, C.; Wang, M. Macroscopic and microscopic analysis of particle flow in direct shear mechanical characteristics of rock structural surface. *Chin. J. Comput. Mech.* **2023**, *40*, 237–248. (In Chinese)
41. Zhou, J.L. Study on Shear Characteristics of Rock-Mortar Heterogeneous Structural Plane. Ph.D. Thesis, Nanchang University, Nanchang, China, 2022. (In Chinese).
42. Kang, Y.S.; Hou, C.C.; Liu, B.; Bai, W. Influence of water content on the shear strength of rock joints with clay-rich fillings. *Rock Mech. Rock Eng.* **2023**, *56*, 1437–1449. [CrossRef]
43. Cao, Y.; Zhang, Y.Y.; Liu, Z.; Bao, M. An experimental study of the effects of filling degree on shear behavior and acoustic emission characteristics of kaolinite-filled granite joints. *Ksce. J. Civ. Eng.* **2024**, *28*, 2966–2981. [CrossRef]
44. Krahn, J.; Morgenstern, N.R. The ultimate frictional resistance of rock discontinuities. *Int. J. Rock Mech. Min.* **1979**, *16*, 127–133. [CrossRef]
45. He, Z.G.; Wilson, S.B.; Monjezi, M.; Tran, T.T. Estimating brazilian tensile strength of granite rocks using metaheuristic algorithms-based self-organizing neural networks. *Rock Mech. Rock Eng.* **2024**, *57*, 4653–4668. [CrossRef]